Dispersion-Relation Fluorescence Spectroscopy

Ru Wang,[1] Lei Lei,[2] Yingxiao Wang,[2] Alex J. Levine,[3,4] and Gabriel Popescu[5,*]

[1]*Quantitative Light Imaging Laboratory, Department of Mechanical Science and Engineering, Beckman Institute for Advanced Science and Technology, University of Illinois at Urbana-Champaign, Urbana, Illinois 61801, USA*

[2]*Department of Bioengineering, University of Illinois at Urbana-Champaign, Urbana, Illinois 61801, USA*

[3]*Department of Chemistry and Biochemistry, University of California at Los Angeles, Los Angeles, California 90095, USA*

[4]*Department of Physics and Astronomy, University of California at Los Angeles, Los Angeles, California 90095, USA*

[5]*Quantitative Light Imaging Laboratory, Department of Electrical and Computer Engineering, Beckman Institute for Advanced Science and Technology, University of Illinois at Urbana-Champaign, Urbana, Illinois 61801, USA*

(Received 16 March 2012; published 2 November 2012)

Because of its ability to study specifically labeled structures, fluorescence microscopy is the most widely used technique for investigating live cell dynamics and function. Fluorescence correlation spectroscopy is an established method for studying molecular transport and diffusion coefficients at a fixed spatial scale. We propose a new approach, dispersion-relation fluorescence spectroscopy (DFS), to study the transport dynamics over a broad range of spatial and temporal scales. The molecules of interest are labeled with a fluorophore whose motion gives rise to spontaneous fluorescence intensity fluctuations that are analyzed to quantify the governing mass transport dynamics. These data are characterized by the effective dispersion relation. We report on experiments demonstrating that DFS can distinguish diffusive from advection motion in a model system, where we obtain quantitatively accurate values of both diffusivities and advection velocities. Because of its spatially resolved information, DFS can distinguish between directed and diffusive transport in living cells. Our data indicate that the fluorescently labeled actin cytoskeleton exhibits active transport motion along a direction parallel to the fibers and diffusive in the perpendicular direction.

DOI: 10.1103/PhysRevLett.109.188104 PACS numbers: 87.16.Ln, 87.64.kv

Trafficking inside live cells is the result of both passive diffusion and active or molecular-motor-driven processes (see, e.g., Ref. [1]). In order to understand intracellular trafficking, one must be able to distinguish these types of dynamics with sufficient spatial and temporal resolution so as to identify the structure of intracellular transport networks and monitor their changes over the course of the cell cycle. Experimentally, this task is challenging due to the multitude of temporal and spatial scales involved. Diffusion of fluorescently tagged molecules has been studied successfully by fluorescence correlation spectroscopy [2–7] and fluorescence recovery after photobleaching (FRAP) [8–11]. In this case, the temporal scales are in the microsecond to millisecond range and the spatial scale is fixed by the excitation beam size. Image correlation spectroscopy (ICS) [12], spatiotemporal image correlation spectroscopy (STICS) [13], and raster image correlation spectroscopy (RICS) [14] have been successfully developed to extract information about fluorophore transport. STICS complements ICS in the sense that it allows measuring the direction of the velocity, in addition to its magnitude. RICS extends ICS to faster diffusion temporal scales. Note that all these methods use confocal scanning imaging.

For studying the transport of larger objects in the cell, e.g., organelles and vesicles, particle tracking has been used successfully [15–17]. However, the cell contains many extended objects or continuous media, such as actin cytoskeleton, which, when viewed on scales large compared to its mesh size, cannot be resolved into separately traceable objects. For this reason, the spatiotemporal fluctuations of such continuous media cannot be investigated by particle tracking. In response to the challenge presented by having to track intracellular dynamics of a broad range of spatial and temporal scales, we have recently developed a label-free method that can be used to study transport in live cells over a broad range of spatiotemporal scales [18,19]. This technique uses quantitative phase imaging [20], works with intrinsic contrast, and, thus, can be used indefinitely without restrictions due to photobleaching or phototoxicity. However, it lacks specificity; i.e., it cannot report on the transport of a specific chemical species or structures.

In this Letter, we propose a fluorescence imaging approach for studying the dynamics of specific structures, both continuous and discrete. This method, referred to as dispersion-relation fluorescence spectroscopy (DFS), uses data collected via time-resolved fluorescence full-field imaging. Therefore, unlike fluorescence correlation spectroscopy or FRAP, DFS renders temporal as well as spatial information. Because it operates in the frequency domain, DFS is complementary to other measurements developed for the same purpose, such as ICS [12], STICS [13], and RICS [14]. Analyzing the frequency ($\mathbf{k}$-ω) domain,

i.e., the dispersion relation of the dynamic transport, is ideal for understanding the physical phenomenon because it directly relates to the governing equation of motion. This allows studying the dynamic properties of intracellular transport in a scale dependent manner. For example, as detailed below, we are able to identify directed and diffusive transport at different spatial scales in living cells.

From the 3D fluorescence data (x, y, t), we calculate $\Gamma(q)$, the wave-number-dependent decay of temporal correlations in the fluorescence signal. The $\Gamma(q)$ curve is a fundamental characteristic of the transport phenomenon under investigation. We fit this dispersion relation using a model based on the diffusion-advection equation, but one in which we assume that the decay of correlations results from an incoherent sum of the advective (i.e., actively driven) motion of many different intracellular elements, such as vesicles or organelles with a distribution of advection velocities. This leads to an expression for the normalized density autocorrelation function of the form

$$g(q, \tau) = e^{i\mathbf{v}_0 \cdot \mathbf{q}\tau} e^{-\Delta v q \tau - D q^2 \tau} \tag{1a}$$

and the decay rate

$$\Gamma(q) = \Delta v q + D q^2. \tag{1b}$$

In Eqs. (1a) and (1b), $q = |\mathbf{q}|$ is the wave number and D is the diffusion constant of cargoes in the intracellular medium. In order to generate the observed linear-in-q decay rate of correlations, we assume a Lorentzian distribution of advection velocities with a mean v_0 and a width $\Delta\nu$.

In order to further validate this interpretation of the data, we demonstrate DFS on standard samples. We recorded time lapses of fluorescently labeled polystyrene beads under both Brownian motion [Figs. 1(a) and 1(b)] and drift [Figs. 1(c) and 1(d)]. These 1.2 μm diameter fluorescent beads were suspended in water between two cover slips and imaged under fluorescence microscopy at acquisition rates of 23 Hz [Fig. 1(a)] and 0.2 Hz [Fig. 1(c)], up to 256 frames and 128 frames, respectively. Figures 1(b) and 1(d) show the trajectories of individual beads corresponding to Figs. 1(a) and 1(c), respectively.

The mean-squared displacements (MSD) and DFS signals associated with the particles in Fig. 1 are shown in Fig. 2. The MSD for the Brownian particles [Fig. 1(a) and 1(b)] were obtained by averaging the trajectories of 229 particles. Figure 2(a) shows a linear fit of this MSD, which yields a diffusion coefficient $D = 0.27 \pm 0.05$ μm^2/s. In order to compute the dispersion relation $\Gamma(q_x, q_y)$ from the fluorescence movie [Fig. 1(a)], we first performed the spatial Fourier transform of each frame, then calculated the temporal bandwidth Γ at each spatial frequency (q_x, q_y). The $\Gamma(q_x, q_y)$ map is shown in Fig. 2(b). We then performed the azimuthal average to obtain the radial profile $\Gamma(q)$, $q = \sqrt{q_x^2 + q_y^2}$. This experimental curve exhibits the expected q^2 dependence associated with diffusion [Fig. 2(c)]. The resulting diffusion coefficient is $D = 0.21 \pm 0.04$ μm^2/s and compares very well the value obtained via particle tracking.

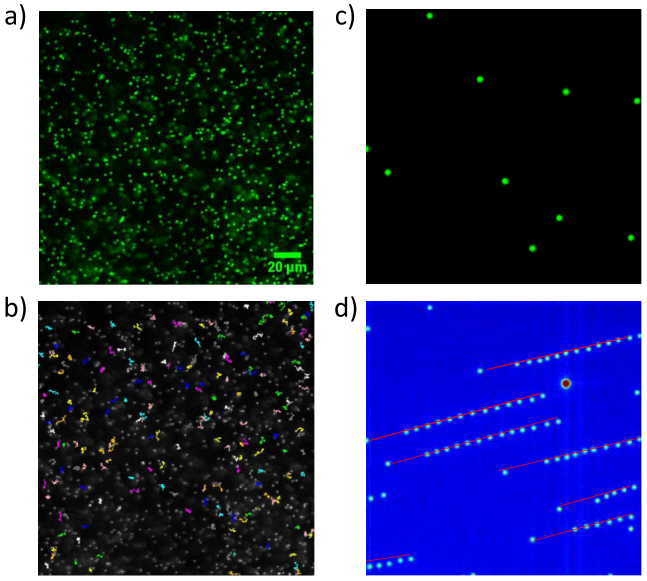

FIG. 1 (color online). (a) Fluorescence images of 1.2 μm polystyrene fluorescence beads in water under Brownian motion. (b) Trajectories of individual beads in (a). (c) Fluorescence images of 1.2 μm polystyrene fluorescence beads drifting from left to the right. (d) Trajectories of individual beads in (c).

For the case of the drift motion shown in Fig. 1(c), the squared displacements along the x direction, $\langle \Delta x(\tau)^2 \rangle$, and the y direction, $\langle \Delta y(\tau)^2 \rangle$, are shown in Fig. 2(d). The resulting components of the drift velocity are $v_x = 32.5$ μm/s, $v_y = 8.8$ μm/s, obtained by fitting a quadratic curve. This drift velocity produces a shift in the power spectrum at frequency $\omega(\mathbf{q}) = v_x q_x + v_y q_y$, which is essentially a q-dependent Doppler frequency shift. We projected angular frequency ω versus wave vector components q_x [Fig. 2(e)] and q_y [Fig. 2(f)]. The corresponding slope yields the drift velocity $v_x = 33.3$ μm/s and $v_y = 9.1$ μm/s, which compare very well with the results of particle tracking.

To prove that DFS works equally well for live cells, we performed experiments in S2 drosophila cells, whose peroxisomes were labeled with green fluorescent protein (GFP). The images were acquired at the rate 1 s per frame up to 2 min with epifluoresce microscopy, as shown in Fig. 3(a). MSD of peroxisomes were calculated after their trajectories were recorded with the ImageJ software, as shown in Fig. 3(b). The linear fit of MSD yields the diffusion coefficients $D = (7 \pm 6) \times 10^{-3}$ μm^2/s [Fig. 3(d)]. We applied DFS to the acquired images and found that the motion of peroxisome was diffusive at time scales of the order of seconds, with $D = (9 \pm 1) \times 10^{-3}$ μm^2/s [Fig. 3(b)], which agrees with that obtained from particle tracking. Thus, DFS can be easily implemented to study motions of discrete particles in live cells, without the need for particle tracking.

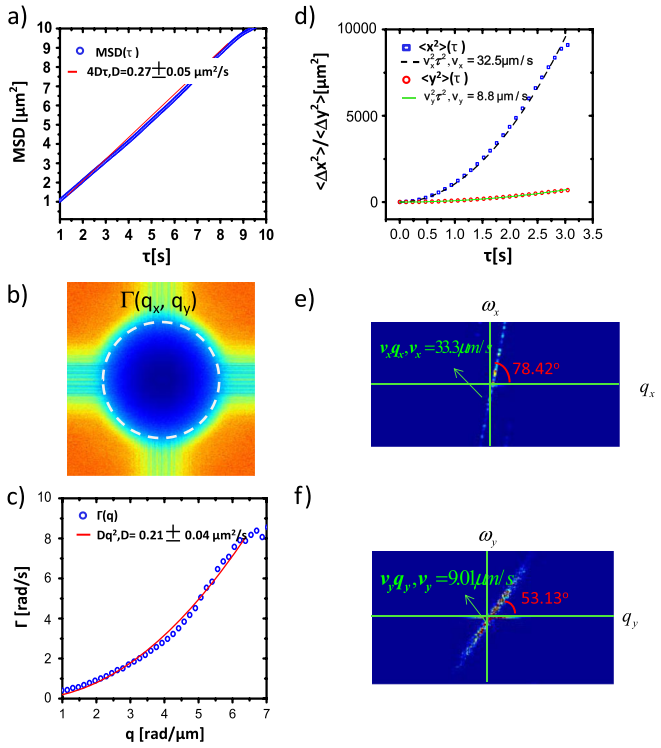

FIG. 2 (color online). Mean-squared displacement (MSD) obtained by tracking individual beads in Fig. 1(a). (b) Decay rate versus spatial mode, $\Gamma(\mathbf{q_x}, \mathbf{q_y})$, associated with the beads in (a). The dashed ring indicates the maximum q values allowed by the resolution limit of the microscope. (c) Azimuthal average of data in (b) to yield $\Gamma(q)$. The fits with the quadratic function yield the value of the diffusion coefficient as indicated. (d) Mean-squared displacement along the x direction and the y direction of beads in Fig. 1(c). (e) Temporal frequency versus spatial frequency. The slope yields the drifting velocity along the x direction. (f) Temporal frequency versus spatial frequency. The slope yields the drifting velocity along the y direction.

Note that, since DFS relies on analyzing fluctuations in the density of fluorophores rather than particle tracking, it applies equally well to continuous mass distributions, such as cytoskeletal structures. To explore such a physical problem, we studied mouse embryonic fibroblasts with their actin cytoskeleton labeled with GFP, as shown in Fig. 4(a). The actin bundles are clearly visible, aligned along the line θ_1. We acquired 256 fluorescence images at a rate of 1 frame per second. The inset of Fig. 4(b) shows the dispersion map, $\Gamma(q_x, q_y)$, which is calculated from those acquired images. Clearly, this dispersion map is no longer isotropic, which is due to the fact that the transport in directions parallel and perpendicular to the actin bundles differs. We identify from the images the directions parallel θ_1 and perpendicular θ_2 to the actin bundles and determine the dispersion curves for motion projected onto these axes. These dispersion relations are plotted on a logarithmic scale in Fig. 4(b). As might be expected, the results indicate that the transport along the actin fibers is directed, as the dispersion curve $\Gamma(q)$ displays q^1 dependence.

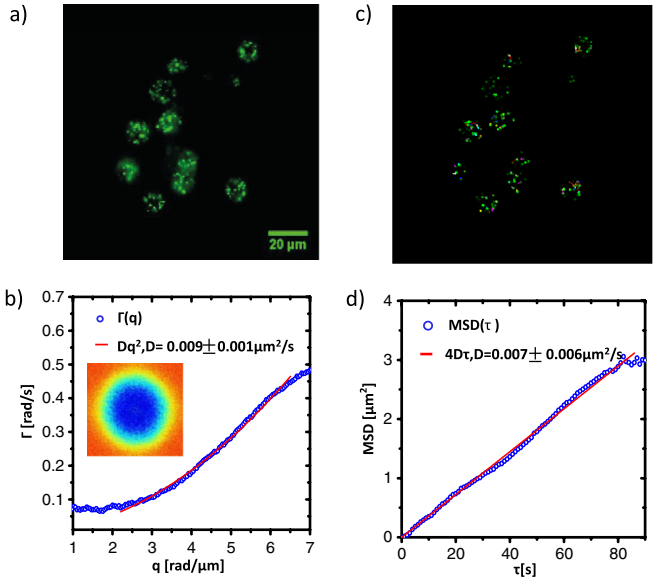

FIG. 3 (color online). Fluorescence images of culture of S2 drosophila cells whose peroxisomes were labeled with GFP. (b) Dispersion curve measured for the cell in (a). The quadratic curve fitting indicates dominant diffusion motion and the fitting coefficients yields the diffusion coefficient. Inset shows the $\Gamma(q_x, q_y)$ map. (c) Trajectories of peroxisomes in (a). (d) MSD obtained tracking the trajectories of peroxisomes. The linear relationship indicates diffusive motion, and the fitting coefficient gives rise to the corresponding diffusion coefficient.

In contrast, the transport perpendicular to the actin fibers is dominated by diffusion, as indicated by the q^2 dependence. These findings are consistent with the well-known phenomenon of "treadmilling" in which seemingly stable actin filaments are actually continually polymerizing at one end and depolymerizing at the other [21–23]. This active process leads to directed 1D transport of actin monomers down the filaments. Transport of actin monomers

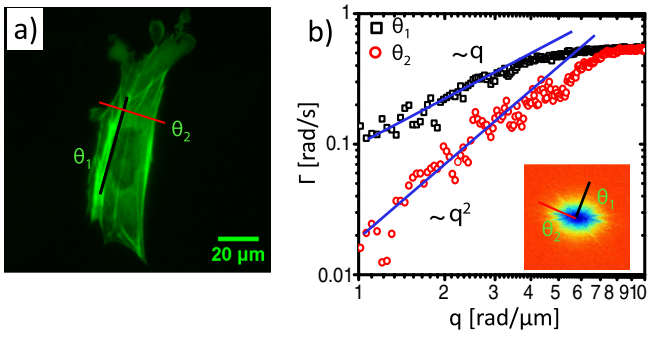

FIG. 4 (color online). (a) Fluorescence images of culture of mouse embryonic fibroblast whose actin was labeled with GFP. (b) Dispersion curve measured for the cell in (a). The black square and red circle curves indicate directed motion and diffusion along θ_1 and θ_2 direction, respectively. The blue lines on top of black and red curves denote their q^1 and q^2 dependence. Inset shows the $\Gamma(q_x, q_y)$ map associated with (a).

perpendicular to the fiber direction, however, does not result from this driven process so that mass transport along θ_2 must be controlled by thermal diffusion.

The reason that q and q^2 curves flatten at the far right part is due to the limited acquisition rate (the Γ range is limited at high values). At that small scale (high q part), the fast dynamics is not sampled fast enough due to the finite frame rate. We kept the acquisition rate low purposely to reduce the amount of exposure and the probability of photobleaching. By doing this, we can distinguish two modes of transport mechanism in the slow dynamics or large scale (low q part). While photobleaching is an important photochemical phenomenon which usually complicates the biological observation and is especially problematic in time-lapse microscopy, it can also be exploited to study the diffusion of molecules in approaches such as FRAP. In this Letter, we simplified the investigation by keeping low exposure, to the point where photobleaching effects are negligible. Thus the signals we observe fully represent the movement of fluorophores and cellular components that they attach to.

In summary, in this Letter we proposed dispersion-relation fluorescence spectroscopy (DFS) to study full-field fluorescence signal fluctuations caused by mass transport. The specific structures of interest are labeled with a fluorophore whose motions give rise to fluorescence intensity fluctuations that are further analyzed to quantify the governing molecular mass transport dynamics. These data are characterized by the effective dispersion relation in the form of a power law, $\Gamma(q) \sim q^{\alpha}$, which describes the relaxation rate of the spatial mode q ($1/\Gamma$ describes the characteristic time of moving particles to travel a $1/q$ mean distance). This dispersion should not be confused with optical dispersion. "Spectroscopy" refers to measuring spatiotemporal frequencies associated with mass transport and should not be confused with optical spectroscopy.

We have demonstrated that DFS can distinguish diffusive from directed (or advective) motion both in a model system where we were able to independently confirm the values of the diffusion constant and advection velocity extracted via DFS. Turning to cellular systems, we found that DFS can be used to make similar distinctions in intracellular mass transport. By studying the transport of monomeric actin in an oriented filament network, we were able to use DFS to observe directed transport along the filaments, consistent with treadmilling, and diffusive transport in the direction perpendicular to them.

Measuring the dispersion relation itself informs us about the spatial scales at which each of the two types of transport, diffusion and advection, is dominant. This description comes naturally because each spatial frequency is characterized by a specific temporal frequency. In the k-ω representation, the two regimes of transport are directly separated even though their respective time constants may differ by orders of magnitude [see, e.g., Fig. 4(b)]. On the other hand, the space-time analysis (correlation calculations) of ICS, RICS, and STICS gives an average effect over all frequencies. In this case, mathematically the fitting function is a temporal convolution between the diffusive and advective terms. Thus, the two contributions overlap in this representation. Unless they have comparable correlation times, the diffusive and directed transport cannot be readily distinguished (Ref. [13] discusses this issue extensively). Furthermore, the frequency domain representation automatically excludes the effects of the static structures in the specimen ($\omega = 0$ contributions), which was discussed in detail by Brown *et al.* [24]. Finally, DFS works with full-field fluorescence imaging (not confocal), which allows collecting data from all points simultaneously and simplifies the analysis.

DFS can be used with particles that cannot be individually resolved, i.e., that are smaller than the diffraction spot of the microscope, as long as the particles travel over distances larger than the diffraction spot. This is typically the case of interest when studying mass transport in live cells. The capability of performing these measurements in a live system provides a new window into the physics of out-of-equilibrium systems. Currently, we are using DFS to study the cytoskeleton dynamics under the influence of various protein-motor inhibitors. In addition to quantifying transport characteristics of molecules, in principle DFS is also capable of estimating the number of fluorescent molecules that contribute to each motion (spatial) component. In order to estimate quantitatively the concentration of fluorescent molecules, we need to perform a series of calibrations, which is the subject of our future work.

This research was supported by the National Science Foundation: CBET 0846660 CAREER (G. P.), CBET 1040462 MRI (G. P.), CBET-0939511 STC (G. P. and Y. W.), NIH HL098472 (Y. W.), and NSF DMR-1006162 (A. J. L.).

*gpopescu@illinois.edu

[1] N. Segev, *Trafficking Inside Cells: Pathways, Mechanisms, and Regulation* (Landes Bioscience, Austin, TX, 2009).
[2] D. Magde, W. W. Webb, and E. Elson, Phys. Rev. Lett. **29**, 705 (1972).
[3] M. A. Digman and E. Gratton, Wiley Interdiscip. Rev.: Syst. Biol. Med. **1**, 273 (2009).
[4] H. M. Chen, E. Rhoades, J. S. Butler, S. N. Loh, and W. W. Webb, Proc. Natl. Acad. Sci. U.S.A. **104**, 10 459 (2007).
[5] U. Haupts, S. Maiti, P. Schwille, and W. W. Webb, Proc. Natl. Acad. Sci. U.S.A. **95**, 13 573 (1998).
[6] D. Lumma, S. Keller, T. Vilgis, and J. O. Radler, Phys. Rev. Lett. **90**, 218301 (2003).
[7] K. Bacia, S. A. Kim, and P. Schwille, Nat. Methods **3**, 83 (2006).
[8] D. Axelrod, D. Koppel, J. Schlessinger, E. Elson, and W. Webb, Biophys. J. **16**, 1055 (1976).

[9] J. Yao, K. M. Munson, W. W. Webb, and J. T. Lis, Nature (London) **442**, 1050 (2006).
[10] L. Y. Wang, Y. L. Wang, Y. F. Han, S. C. Henderson, R. J. Majeska, S. Weinbaum, and M. B. Schaffler, Proc. Natl. Acad. Sci. U.S.A. **102**, 11 911 (2005).
[11] J. C. Politz, E. S. Browne, D. E. Wolf, and T. Pederson, Proc. Natl. Acad. Sci. U.S.A. **95**, 6043 (1998).
[12] N. O. Petersen, P. L. Hoddelius, P. W. Wiseman, O. Seger, and K. E. Magnusson, Biophys. J. **65**, 1135 (1993).
[13] B. Hebert, S. Costantino, and P. W. Wiseman, Biophys. J. **88**, 3601 (2005).
[14] M. A. Digman, C. M. Brown, P. Sengupta, P. W. Wiseman, A. R. Horwitz, and E. Gratton, Biophys. J. **89**, 1317 (2005).
[15] M. T. Valentine, P. D. Kaplan, D. Thota, J. C. Crocker, T. Gisler, R. K. Prud'homme, M. Beck, and D. A. Weitz, Phys. Rev. E **64**, 061506 (2001).
[16] J. H. Shin, M. L. Gardel, L. Mahadevan, P. Matsudaira, and D. A. Weitz, Proc. Natl. Acad. Sci. U.S.A. **101**, 9636 (2004).
[17] T. A. Waigh, Rep. Prog. Phys. **68**, 685 (2005).
[18] R. Wang, Z. Wang, L. Millet, M. U. Gillette, A. J. Levine, and G. Popescu, Opt. Express **19**, 20571 (2011).
[19] R. Wang, Z. Wang, J. Leigh, N. Sobh, L. Millet, M. U. Gillette, A. J. Levine, and G. Popescu, J. Phys. Condens. Matter **23**, 374107 (2011).
[20] G. Popescu, *Quantitative Phase Imaging of Cells and Tissues* (McGraw-Hill, New York, 2011).
[21] Y. Aratyn-Schaus and M. L. Gardel, Science **322**, 1646 (2008).
[22] C. E. Chan and D. J. Odde, Science **322**, 1687 (2008).
[23] T. D. Pollard and J. A. Cooper, Science **326**, 1208 (2009).
[24] C. M. Brown, R. B. Dalal, B. Hebert, M. A. Digman, A. R. Horwitz, and E. Gratton, J. Microsc. **229**, 78 (2008).